The Relation of Seafloor Voltages to Ocean Transports in North Atlantic Circulation Models: Model Results and Practical Considerations for Transport Monitoring*

Á. H. FLOSADÓTTIR+ AND J. C. LARSEN

Pacific Marine Environmental Laboratory, National Oceanic and Atmospheric Administration, Seattle, Washington

J. T. SMITH#

Department of Geophysics, University of Washington, Seattle, Washington

(Manuscript received 1 May 1995, in final form 8 November 1996)

ABSTRACT

Motionally induced voltage differences offer one of the few observational methods sensitive to changes in large-scale ocean transports. They present a useful contrast to most oceanographic data by virtue of their natural spatial integration, temporal continuity, and potentially long duration. However, widespread oceanographic use of the voltages observable with seafloor cables has been impeded by uncertainties of interpretation. Interpretation in terms of volume transport fluctuations has proved successful in the Straits of Florida and for a short cable in the easternmost part of the Bering Strait. Still, a number of older experimental studies resulted in disappointment, the Bering Strait work has been little known, and the Florida success might be a special case. The question considered in this paper is: Does a linear relationship between net transport and voltage difference fluctuations hold for long, open-ocean cables? This question is addressed by using a numerical model based on two years of results from the WOCE Community Modeling Effort, which simulated the wind-driven and thermohaline circulation in the North Atlantic using mean monthly winds and realistic topography with a resolution sufficient to permit mesoscale eddies. The model includes the effects of spatial and temporal variations of seawater temperature and salinity, electric current loops, the effects associated with the meandering of ocean currents over realistic topography and sediment thickness, realistic earth conductivity, and the spatially varying geomagnetic field. The main result is that the relationship between voltage and net cross-cable transport fluctuations can be remarkably linear over long distances. In view of the difficulties of long-term, large-scale transport monitoring by other methods, the implication of this work is that well chosen and carefully interpreted voltage observations hold great promise. This should be explored through renewed modeling, observation, and interpretation efforts.

1. Introduction

Continuous observation of large-scale net ocean transport variations on timescales ranging from weekly to decadal would be useful for monitoring the ocean general circulation and for understanding its role in climate variability and change. Such observations would also be useful for general circulation model evaluation and improvement. However, many traditional methods measure only part of the flow field, and most are highly intermittent in either space or time. Combining the necessary spatial coverage with the temporal duration and resolution needed to monitor the net transports presents a formidable task.

Motionally induced voltage differences are sensitive to the complete flow field and to the full depth. Their spatial integration, high temporal resolution, and potentially long duration are highly complementary to the majority of other oceanographic data. The conventional interpretation of voltage data is in terms of volume transport. More general forms of interpretation may prove useful, for instance using voltages to constrain a linear combination of volume, heat, and salinity flux in numerical representations of the ocean; combination with inverted echo sounders to resolve the first two dynamical modes (Luther and Chave 1993) or interpretation in terms of the heat and salinity fluxes for cables that straddle recirculating or estuary exchange flow. In this paper, however, we use a numerical model of the earth and ocean to evaluate the conventional interpretation in terms of volume transport. The question addressed is:

*Pacific Marine Environmental Laboratory Contribution Number 1764.

+Current affiliation: Joint institute for the Study of Atmosphere and Ocean, University of Washington, Seattle, Washington.

#Current affiliation: Department of Materials Science and Mineral Engineering, University of California, Berkeley, Berkeley, California.

Corresponding author address: Dr. Agusta H. Flosadóttir, NOAA/PMEL,7600 Sand Point Way, Seattle, WA 98115.
E-mail: agusta@pmel.noaa.gov

How widely does a linear relationship between net transport and voltage difference fluctuations hold for open-ocean cables?

2. Motional induction

Motional induction arises when the electrically conducting ocean flows across the earth's magnetic field. The theory has been developed by many authors, among them Longuet-Higgins et al. (1954), Sanford (1971), Robinson (1976), Chave and Luther (1990), and Larsen (1992). We consider timescales longer than one month or so, ignoring displacement currents, self induction, and mutual induction (see section 4). With these assumptions, Maxwell's equations can be reduced to a time-independent continuity equation for the electric current and Ohm's law for a moving medium,

$$\nabla \cdot \mathbf{j} = 0 \tag{1}$$

$$\mathbf{j} = \sigma(\mathbf{E} + \mathbf{v} \times \mathbf{F}). \tag{2}$$

Here $\mathbf{j}$ is the electric current density, σ is the electric conductivity of the earth and ocean, $\mathbf{E}$ is the electric field in a seabed frame of reference, $\mathbf{v}$ is the water velocity, and $\mathbf{F}$ is the steady geomagnetic field, geomagnetic fluctuations, and the magnetic fields caused by $\mathbf{j}$ being neglected. For large-scale slowly varying ocean currents, the ocean is to first order surrounded by insulators, large-scale electric currents are negligible, and Ohm's law is satisfied by electric charge buildup until the cross-stream electrostatic forces balance the depth-integrated force due to the seawater's motion across the geomagnetic field (Fig. 1a).

For the large-scale circulation, where the flow field varies on scales much greater than the ocean depth, the horizontal component of the electric field is essentially the same from the sea surface to the seafloor. Furthermore, the problem is quasi-static so that the electric field can be derived from a scalar potential ϕ by

$$\mathbf{E} = -\nabla\phi. \tag{3}$$

The line integral of the electric field is then path independent, and the voltage difference between two endpoints is given by

$$\Delta\phi = -\int_{\substack{\text{any path between}\\ \text{the endpoints}}} \mathbf{E}\cdot\mathbf{dl}. \tag{4}$$

This voltage difference can be measured with a voltmeter whose leads consist of insulated cables with endpoints in contact with the local ground or seawater (Fig. 1b). For measurements of the local electric field, ''electrometers'' are used to observe the voltage differences over the span of relatively short cables or water-filled pipes, usually a few meters (e.g., Filloux 1987; Webb et al. 1985; Petitt et al. 1994; Luther and Chave 1993). For voltages across longer distances, up to basinwide scales, the modern possibilities include both retired and in-service analog and fiber optic telecommunication cables (e.g., Larsen 1992; Lanzerotti et al. 1993). In-service or discontinued military surveillance cables may also become available. Furthermore, it may be feasible to lay dedicated cables to cover relatively short distances in straits and at circulation choke points.

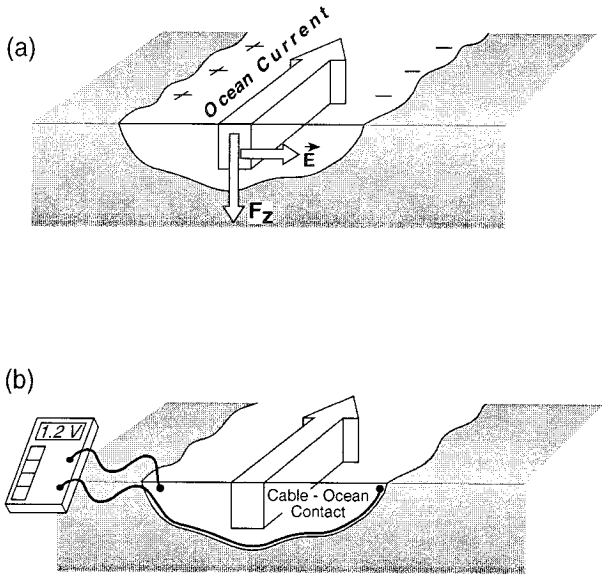

FIG. 1. (a) A sketch of the basic situation for large-scale, low-frequency ocean motions in the deep ocean where sediments can be ignored. F_z is the vertical component of the geomagnetic field (downward in the northern geomagnetic hemisphere), and E is the cross-stream electric field. (b) A sketch of the use of a seafloor cable as voltmeter lead to sense motionally induced voltage differences in the ocean.

3. Approximate relationships and questions of cable voltage interpretation

When depth-integrated electric currents are neglected, which is equivalent to the neglect of large-scale electric current loops, an approximate form for the horizontal electric field averaged over an area of a few times the water depth (Sanford 1971; Chave and Luther 1990) is given by

$$\mathbf{E}_H = -\bar{\mathbf{v}}^* \times \hat{\mathbf{z}} F_z, \tag{5}$$

where the conductivity weighted velocity, denoted $\bar{\mathbf{v}}^*$ by Sanford (1971), is given by the ratio $\bar{\mathbf{v}}^* = \mathrm{C}/\tau$; C is the electric conductivity flux,

$$\mathrm{C} = \int_{\substack{\text{sea}\\ \text{floor}}}^{\substack{\text{sea}\\ \text{surface}}} \sigma\mathbf{v}\, dz, \tag{6}$$

and τ is the electric conductance of the sea plus the uppermost part of the seabed,

$$\tau = \int_{\substack{\text{resistive}\\ \text{rock}}}^{\substack{\text{sea}\\ \text{surface}}} \sigma\, dz. \tag{7}$$

The integration is traditionally assumed to include any sediment cover and the most conductive crustal rocks down to an effectively insulating layer. The integral should include that part of the seabed through which electric shorting by localized vertical loops is important.

In much of the World Ocean, seawater conductivity can be approximated by a constant plus smaller terms linear in the temperature and the salinity. Under the approximations above, the conductivity weighted transport and the electric field are then linear combinations of the depth-integrated volume, heat, and salinity fluxes, so that the voltage between the ends of a cable consists of the alongcable integral of a linear combination of the (usually dominant) volume flux, the heat flux, and the (usually minor) salt flux. Interpretation of voltage data in terms of this linear combination could provide a very useful constraint on numerical representations of the ocean. The traditional way to interpret cable data, however, is in terms of the net volume transport only. This type of interpretation calls for more restrictive approximations. One concern has been voltage variations resulting from the meandering of ocean currents across topography or variable sediment cover. This can cause variations in the amount of electrical shorting by localized electric current loops with return paths through the underlying water column or sediments. This effect is largest where there are large relative changes in the water depth, or in shallow water with rapidly changing sediment cover, and is much smaller in deep water. For long cables, the spatially varying geomagnetic field can produce a similar effect. A second concern has been the influence of spatial and temporal variations in temperature or salinity, and hence in seawater electrical conductivity, changing either the effective conductivity of the flow or the ratio of integrated seawater conductivity to seabed conductance. A third concern has been that shorting by large-scale electric current loops, either with return paths through the ocean or deep into the earth's mantle, might cause voltages unrelated to the local oceanography. Evidence supporting the neglect of nonlocal voltages is provided by the absence of significant nonlocal signals at subtidal frequencies in horizontal electric field measurements in the Sargasso Sea (Cox et al. 1980), the northeast Pacific (Luther et al. 1991), and in the Tasman Sea (Lilley et al. 1986). Measurements from the North Atlantic, the SYNOP experiment (Luther and Chave 1993) and off the Bahamas (Sanford et al. 1995; Chave et al. 1997) are consistent with this interpretation, as are, on the whole, our model results (Flosadóttir et al. 1997). The possibility has been kept open, however, by theoretical and numerical work (Sanford 1971; Stephenson and Bryan 1992; see further discussion in Flosadóttir et al. 1997), and by the sparse coverage of experimental data. A final and practical concern has been that prohibitively expensive independent transport data might be required to establish a linear relationship and determine the calibration factor that converts voltage to transport fluctuations. All these concerns have been open questions for many years, especially for open-ocean cables.

The fundamental requirement for interpretation in terms of volume transport to make sense is linearity of the relationship between voltage and transport. When this relationship is a reasonably tightly constrained line, relative voltage fluctuations correspond to relative transport fluctuations. If in addition, the slope can be established, voltages can be translated into absolute transport fluctuations. The value of the slope or ''calibration factor'' depends on where the flow is concentrated relative to the topography, underlying sediments, and magnetic field, as well as on the effective flow temperature and salinity. The calibration problem consists of establishing the linearity of the voltage–transport relation and estimating its slope.

The usefulness of cable voltages for monitoring transports in favorable circumstances, such as in well-defined straits, has by now been thoroughly established by the ongoing work with the cables spanning the Straits of Florida at 27°N (e.g., Sanford 1982; Larsen and Sanford 1986; Spain and Sanford 1987; Leaman et al. 1987; Larsen 1992). A highly linear relationship between voltage and net transport was also established for a cable approximately 9 km long in the eastern Bering Strait (Bloom 1964) and, very recently, by comparison with ADCP measurements for a cable across Tsugaru Strait (Rikiishi et al. 1996). A number of older studies, however, (for reviews, see for example Longuet-Higgins 1949; Bullard and Parker 1968; Larsen 1992; and Lanzerotti et al. 1993), suffered from attempts to interpret tidal or time-averaged voltages directly in terms of ocean flows. The tidal timescales were subject to contamination by external signals and by complications due to ocean self-induction, while in the DC limit, interpretation was complicated by cable-ocean contact electrochemical biases and possibly by steady electric currents from the earth's core (see section 4). In the last few years, voltage measurements have been initiated for several cables, mainly in the Pacific (e.g., Chave et al. 1992; Lanzerotti et al. 1993). Some of the work has concentrated on signals of geomagnetic origin, but oceanographic signals have been studied by comparison with pressure, wind stress, and wind stress curl data (e.g., Fujii 1995) and ADCP measurements (Rikiishi et al. 1996). We devote this paper to seeing what a realistic numerical model of the earth and ocean has to contribute to the interpretation of cable voltages in terms of volume transport.

4. Limitations and the useful frequency range

Nonmotional voltages limit the range of periods where cable voltages are useful for ocean circulation studies to the range of periods from a few days up to interannual and inderdecadal scales. At the short period end, external fluctuations such as geomagnetic storms are a significant contribution to cable voltages. The ex-

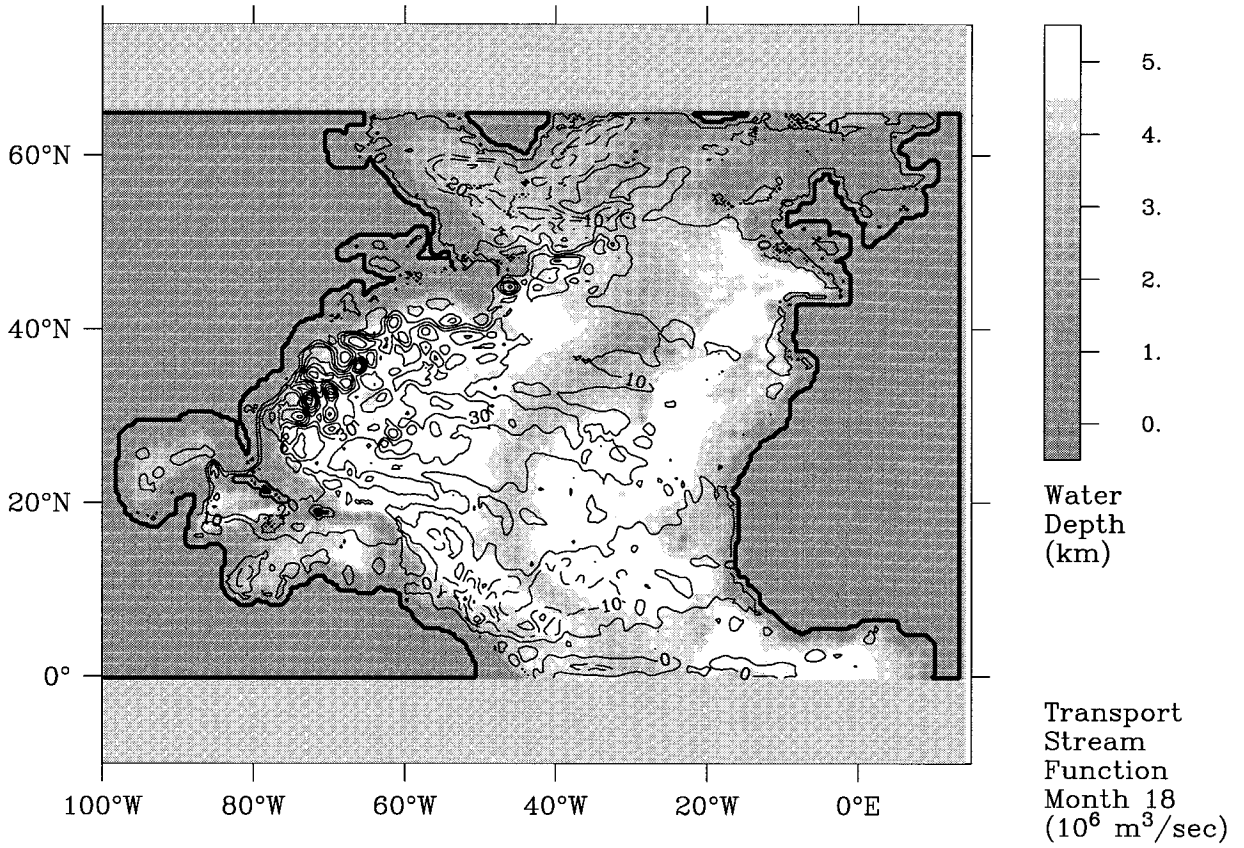

FIG. 2. Contours of the transport streamfunction for the 18th of our 24 CME model months (June of the final model run year). This month was chosen for the illustration to show an example from summer since month 24 (December) was used for a similar illustration in Flosadóttir et al. (1997), where figures showing more of the model ingredients may be found. The contour interval is 10 Sv. Model bathymetry is indicated by shading.

act point where external fields take over depends both on the cable length and the local oceanography. For the Straits of Florida cable, ~100 km long, they were found to become negligible compared with oceanographic signals at periods longer than about 5–10 days, with the crossover between motionally and externally induced spectra near 5-day periods (Larsen 1992). For extremely long cables, trans-Pacific cables, for instance, external fields can be detected out to longer periods on the order of 30 days. This is because the oceanic flow field is characterized by spatial scales smaller than those of the external signals so that relatively more of the ocean-induced signal is integrated out by a very long cable (Chave et al. 1992; Fujii et al. 1995). In many cases, removal of external signals can be accomplished by use of correlations with magnetic field measurements at remote sites (e.g., Larsen 1989; Larsen et al. 1996).

Another limitation at the high-frequency end is our neglect of self and mutual induction. This is appropriate for low frequencies and moderate spatial scales such that the induction number or magnetic Reynolds number, $\omega\mu\sigma L\,H$, is much less than 1. Here σ is the electric conductivity and the length scales L and H depend on the geometry of the flow and the associated electric current loops. Self-induction is believed to be important for the deep-water tides and for basinwide sloshing modes with periods of a few days (cf. Larsen 1968; Chave and Luther 1990). The present study, however, is restricted to timescales longer than one month or so. For a period of 30 days and gyre-scale L and H the induction number is $O(1)$, but by Sanford's (1971) estimate of the relevant length scales it is much smaller. It would be desirable to include self and mutual induction in our model, but for the North Atlantic general circulation we do not expect the error to be large at the periods we are considering.

Nonmotional DC voltages are due to cable–ocean contact electrochemical biases and to any steady electric currents due to dynamo processes in the earth's core (Runcorn 1964; Lanzerotti et al. 1993). These mean that cable voltages are, in general, useful for temporal fluctuations only. Instability of the cable–ocean contacts can be minimized by careful choice of contact locations and by the use of high-quality electrodes (for a review, see Filloux 1987; for a comparison of several types of electrodes in the Straits of Florida, see Larsen 1992). With silver–silver chloride electrodes, drifts in a coastal well were found to be on the order of a millivolt (for dis-

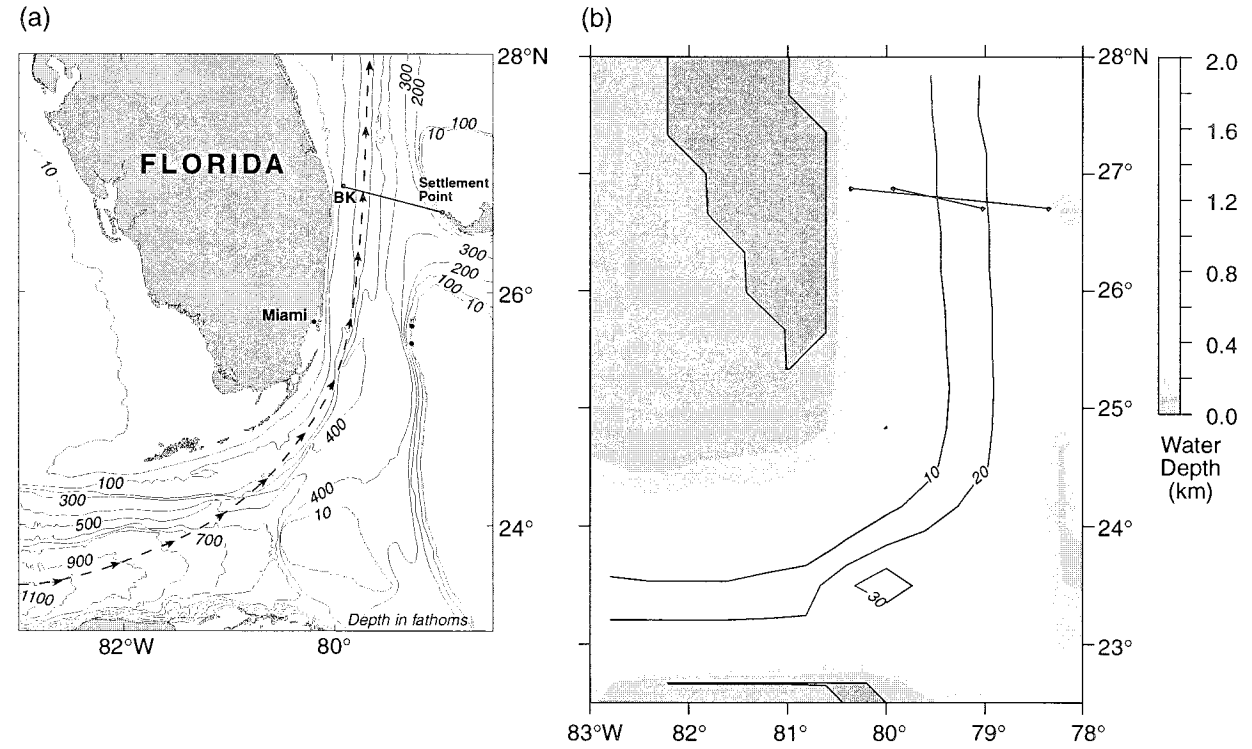

FIG. 3. (a) Map of the Straits of Florida, the cable used for voltage monitoring studies during the 1980s, and axis of the Florida Current (after Larsen 1992). The axis of the Florida Current is represented by a dashed line. (b) Corresponding region in the CME model together with the time-averaged CME transport streamfunction. The shorter cable shown is the same as in (a). The longer ''cable'' links the endpoints used for the model-computed calibration in the text. We have left the N–S coordinates of the endpoints unchanged, but have expanded the E–W coordinates to better span the model strait. Contours of the time-averaged transport streamfunction at 10-Sv intervals are plotted to indicate the location of the main flow.

cussion and time series, see Larsen 1992). On the sea floor, drifts would be expected to be smaller, but this is already much smaller than typical long-cable oceanographic signals, which are on the order of tens or hundreds of millivolts.

5. Our numerical model of flow-induced voltages

Treatment of the electromagnetic theory used in our modeling may be found in the works listed in the introduction, and the details and tests of our computational method are described in Flosadóttir et al. (1997). Ignoring external signals, displacement currents, self and mutual induction, we solve the combination of (1)–(3) for the electric potential. The staggered-grid finite difference scheme is designed to satisfy conservation laws exactly (Visscher 1989) in a way similar to the traditional finite difference schemes for ocean general circulation models (e.g., Bryan 1969). The detailed discretization is obtained by integrating over the gridcells, using Gauss' law to convert volume integrals of the divergence of various quantities into surface integrals of the outward components of $\sigma\mathbf{E}$ and $\mathbf{C} \times \mathbf{F}$, retaining only the vertical component of $\mathbf{F}$. The differential equation is solved in three dimensions, using a 3D conjugate gradient method with incomplete Cholesky decomposition (Smith 1996a,b). We implemented spherical coordinates and adapted the code for our application.

For the flow field, we used the WOCE[1] Community Modeling Effort's first experiment model North Atlantic (Bryan and Holland 1989), the ''CME'' model. This simulated the wind-driven and thermohaline circulation in the North Atlantic using the mean monthly winds of Hellerman and Rosenstein (1983) and realistic topography with resolution sufficient to permit mesoscale eddies. Figure 2 shows the model domain and the bathymetry, as well as one of the monthly ''snapshots'' of the transport streamfunction. These were obtained by filtering and resampling the last two years of the CME model run to yield a simulated 24-month time series. To obtain ocean conductivities and their fluxes, we used the relation of potential to in situ temperatures from Gill (1982) and the relation of conductivity to temperature, salinity, and pressure from Fofonoff and Millard (1983). The seafloor bathymetry was taken from the oceanographic model, and the geomagnetic field was obtained from the 1980 International Geomagnetic Reference Field (this field was appropriate because one of our main

[1] World Ocean Circulation Experiment.

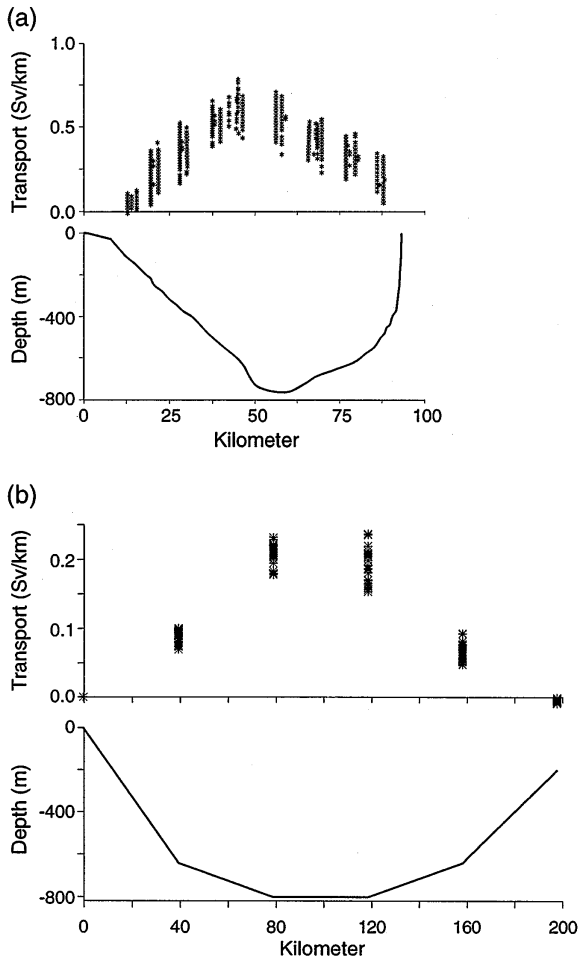

FIG. 4. Channel profile and transport per unit width in the Straits of Florida at 27°N. (a) Empirical data taken from Pegasus profiling at various times over the period 1981–90 (courtesy of Leaman et al. 1987). (b) CME model monthly values for the final two years of the run.

objectives was to compare with the 1980s cable calibration from the Straits of Florida). Sediment thicknesses from seismic data (Emery and Uchupi 1984) were digitized to a 1° grid. Finally, the three-dimensional earth conductivity structure for the upper 40 km was based on the seabed reference model compiled from various sources by Chave et al. (1990). Sediment conductivity profiles were constructed to include the effects of porosity variations with depth and the geothermal gradient (see Flosadóttir et al. 1997). Deeper conductivities were based on data interpretations from the geophysical literature (e.g., Tarits 1994). Since the model includes flow meandering, realistic topography and sediment cover, spatial and temporal seawater temperature and salinity variations, and large-scale electric current loops, all of the effects that have caused uncertainty about cable voltage interpretation are modeled.

Various tests of the numerical model are described in Flosadóttir et al. (1997). Most relevant to this paper is the comparison with the empirical cable calibration in the Straits of Florida at 27°N (Fig. 3). The empirical and simulated calibration factors are shown in Table 1 using the two sediment conductance models of Flosadóttir et al. (1997), which differ everywhere by a factor of 1.1/0.7. In the Straits of Florida, they are roughly consistent with the local determinations of Spain and Sanford (1987) and the cable-based estimate of Larsen (1992), respectively. The agreement with the empirical calibration factor must be considered good given the CME model's imperfect resolution of the straits (Figs. 3 and 4) and the uncertainty in the local sediment conductance (Spain and Sanford 1987; Larsen 1992). The rms misfit is reproduced quite well, presumably to a large extent because the CME model reproduces the relative amount of meandering reasonably well (Figs. 4 and 5).

6. An open ocean example: The Bermuda–New Jersey cable

In the following section, we tabulate numerical calibration results for a large selection of North Atlantic cables. Before presenting those results, however, it is important to look at at least one example in depth. Our aim in this section is to allow the reader to judge the importance of local variables, such as the sediment geology, and the quirks of the particular ocean model. Both are very relevant to the question of how well we can simulate the voltage–transport relationship and how ac-

TABLE 1. Model and experimental cable calibration results for the Straits of Florida at 27°N. The model results labeled ''Grand Bahama'' were obtained using the real-world coordinates of the cable landing at Settlement Point, Grand Bahama Island. For the results labeled ''CME-Bahamas,'' the endpoint was moved farther east within the shallow sea that replaces the Bahamas in the CME model. This was done so that the model cable would better span the actual model channel (cf. text and Figs. 6 and 7). The sediment conductance models labeled ''high'' and ''low'' are the ones discussed in the text and in Flosadóttir et al. (1997).

Calibration method	Cable endpoints	Sediment electric conductance	Correlation coefficient squared	Calibration factor (mV Sv^{-1})
Experimental	Break off Jupiter–Grand Bahama	Real seabed	.94	40.9
Model	Break off Jupiter–Grand Bahama	High	.98	30.4
Model	Break off Jupiter–Grand Bahama	Low	.98	36.4
Model	Break off Jupiter–CME-Bahamas	High	.99	31.9
Model	Break off Jupiter–CME-Bahamas	Low	.99	38.7

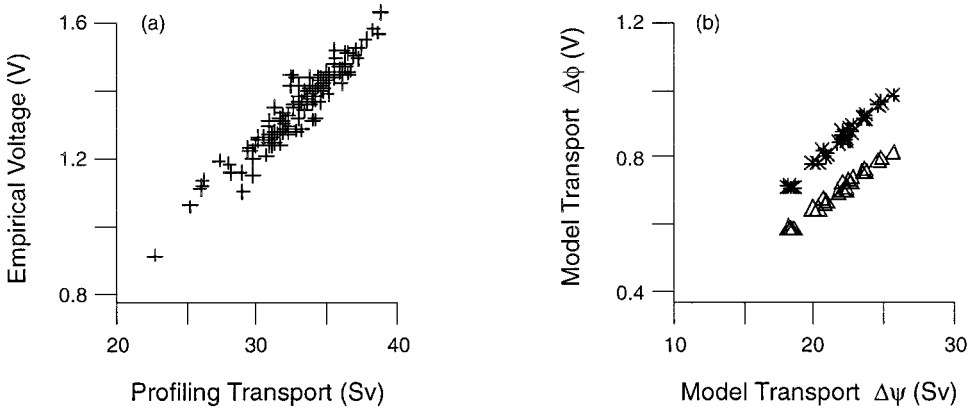

FIG. 5. Empirical and simulated voltage–transport relations for the Straits of Florida at 27°N. (a) Empirical voltage–transport relationship for the abandoned cable in the Straits of Florida (after Larsen 1992). The voltages measured from a cable break off Jupiter Inlet to Settlement Point on Grand Bahama Island over the period 1981–90. Values shown when simultaneous transports were available from Pegasus velocity profiling, the data courtesy of Leaman et al. (1987). The calibration factor (slope) is $24.4 + -0.6$ Sv V^{-1}, the correlation squared is 0.94, and the rms misfit 0.8 Sv. The plot shows a larger scatter than this because transport estimates extrapolated from incomplete profiling data (that is, based on transports extrapolated from acoustic profiling on days when the profiling failed to cover the full channel width) are included in the plot, but are weighted according to completeness for the line fitting (for the details see Larsen 1992). (b) Simulated relationship between the CME model transports and computed voltage difference between two points straddling the wider version of the model Straits of Florida (not the same as the real-world cable endpoints). Stars: the less conductive; triangles: the more conductive sediment model. The numerical calibration (Fig. 5b) was done by fitting a straight line to 24-month time series of simulated transports and voltages based on the CME model. For the correlation, misfit, etc., see Tables 1 and 3.

curately we can estimate deep-water cable calibration factors based on numerical models.

As the concrete example with which to illustrate these questions, we consider the New Jersey–Bermuda Cable (Fig. 6). This cable was laid in 1962 between Manahawkin, New Jersey, and Flatts, Bermuda (U.S. Dept. of Commerce 1991), by AT&T and Cable & Wireless, Ltd. It was retired in 1987, and its shore connections have since been removed. The Bermuda cable provides a good case to test many of the concerns about open-ocean cable voltage–transport linearity and calibration. The region has a pronounced correlation of the most conductive water with poleward flow and vice versa, and fluctuations of this relationship will manifest themselves as calibration factor fluctuations. Sediment conductance uncertainty is less important here than in shallow and heavily sedimented locations such as the Straits of Florida since in deep water the return path for electric current provided by the seabed is only a few percent of the water column's conductance. Nonetheless, while the meanders of the Gulf Stream occur mainly over relatively deep water, the variability associated with recirculations, the deep western boundary current, and the eddy field extends over both the continental slope and the Bermuda Rise. The variations of water depth and sediment cover along the cable path will affect the local conversion factor between electric field and transport, making meandering effects a concern. Furthermore, this cable crosses the western boundary currents in a region where the CME model has difficulty with its Gulf Stream separation (cf. Figs. 6 and 7; see Boening et al. 1996). It therefore provides a good example with which to discuss how a model's shortcomings affect the numerical calibration. Finally, as a decommissioned cable that has lost its shore connections, it provides a context for exploring the possibilities of using underwater instrumentation to monitor the deep-water part of the cable only. To illustrate this, we consider both the voltage across the full-length original cable, and between points about 100 nautical miles offshore at either end (Fig. 6).

Going through the exercise of using back-of-the-envelope methods to estimate extreme bounds on the Bermuda cable calibration factor (appendix) is helpful in developing a sense of how various variables affect the linearity and calibration. Estimated extremes of the local calibration factor based on generous estimates of the range of possible effective depths, sediment conductivities, flow-conductivity correlation factors, and magnetic field values, cover the range of 9–21 mV/Sv (Sv $\equiv 10^6$ m^3 s^{-1}) for flow across the deep water stretch of the Bermuda cable in water deeper than 3 km or so (Table 2, see the appendix for details). Were the flow concentrated over the upper reaches of the continental slope, a similarly estimated range would be roughly 22–52 mV/Sv. It is apparent from comparing these ranges that if the flow were to alternate significantly between the two regions, voltage differences over the whole cable would be unlikely to provide good measures of total transport.

The CME model shows good linearity for our two-

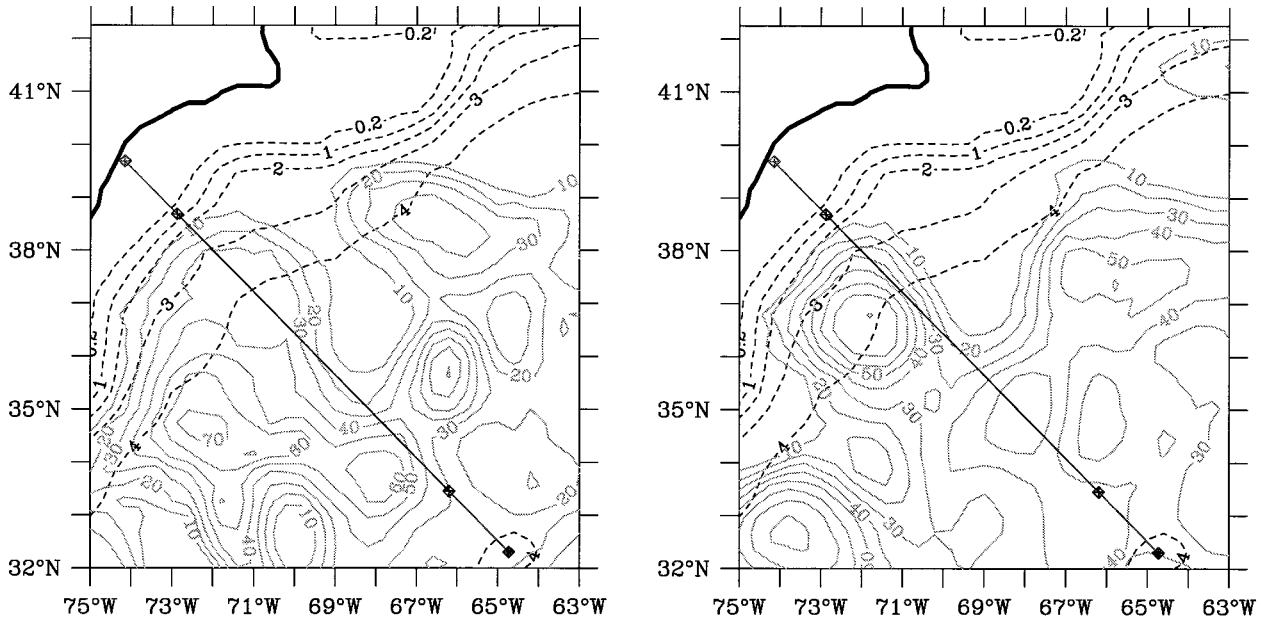

FIG. 6. The New Jersey–Bermuda cable (solid). The cable ends are shown by squares, both for the full length original cable and for a deep water portion terminating about a 100 nautical miles offshort at each end. The CME model coastline is indicated by a heavy line and contours 200 m, 1, 2, 3, and 4 km by dotted, light-colored contours. A snapshot of the CME transport streamfunction is indicated by the solid contours, contour interval 10 Sv. (a) June of the final CME model year. (b) December of the final CME model year.

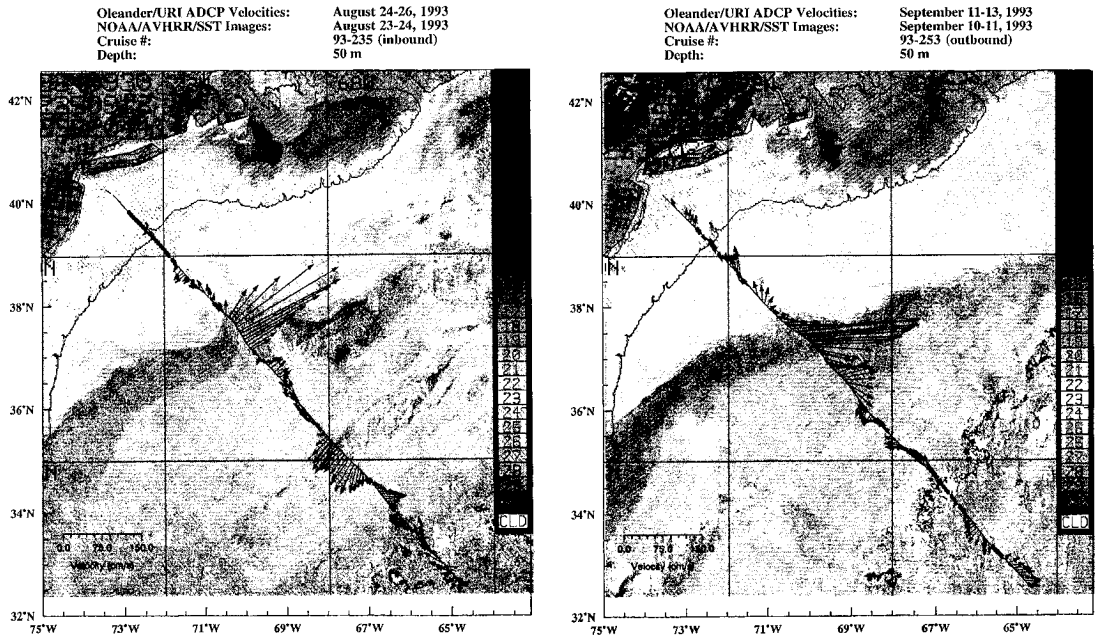

FIG. 7. Flow at 50-m depth from a program of ongoing ADCP measurements from the container ship *Oleander*, with a regular route very close to the Bermuda cable. Stick plots of 10-min (4 km) averaged ADCP velocities at the 50-m depth level superimposed on nearly concurrent NOAA/AVHRR satellite sea surface temperature (SST) images from August (left panel) and September (right panel). Velocities less than the instrument threshold (about 0.01 m s^{-1}) are indicated with a dot. Temperatures (in °C) are indicated in the grayscale (white is cloud cover). The 200-m isobath is indicated by the solid line. The region shown is the same as in the previous figure. After Gottlieb et al. (1994); see also Flagg et al. (1997).

TABLE 2. Model-derived calibration results for the Bermuda–New Jersey cable. Sediment models the same as in Table 1.

Calibration method	Cable endpoints	Sediment electric conductance	Correlation coefficient squared	Calibration factor (mV Sv^{-1})
Estimated extremes	Upper continental slope			22–52
Estimated extremes	Deepest stretch, 3–5-km depth			9–20
Model	New Jersey–Bermuda	High	.86	11.4
Model	New Jersey–Bermuda	Low	.79	12.6
Model	100 n mi offshore only	High	.97	9.4
Model	100 n mi offshore only	Low	.94	9.7

year simulated time series, with a model-derived calibration factor of 11.4–12.6 mV/Sv for the full-length cable and 9.4–9.7 mV/Sv for the deep water part (Table 2). The range represents the two sediment conductance models discussed earlier. The table also shows that by using the deeper, offshore part of the cable only, there is a significant improvement in the voltage–transport correlation. Furthermore, the calibration factor's sensitivity to the sediment assumptions is reduced. The uncertainty due to seabed conductance could be narrowed down further by careful incorporation of more geologic information and seabed conductance estimates from the region. However, it is already small for the deep-water offshore portion of the cable.

For a closer look at the model results, Fig. 8 shows two representations of the simulated data. The left-hand panel shows the 24-month time series of simulated voltage and simulated transport across the deep-water offshore Bermuda cable, scaled to fit on the same plot. The right-hand panel is a scatterplot, following the standard representation of empirical calibration data. In order to keep the figure uncluttered, only results for the more conductive of the two sediment models are shown. The transport fluctuations are well captured by the voltage. The large intersect (the nonzero voltage at zero transport) evident in Fig. 8b is due to the not altogether realistic semistationary recirculation over the slope side of the cable. The inshore and offshore branches of the recirculation cell are situated in different depths of water and over different sediment thickness. This means that the voltage from the two branches fails to cancel at zero net transport.

The rms misfit between the voltage and transport curves in the model is sizeable, 2.4–2.8 Sv (Table 3). A decomposition of the simulated time series by timescales helps sort out the sources of the misfit so that we can evaluate how they correspond with the real world. Figure 9 shows the part of the signal remaining after the time series has been filtered with a 3-month boxcar average, and Fig. 10 shows the slower, filtered variations. The contrast between the extremely good linearity of the month-to-month variations and the poorer linearity and larger misfit of the slower variations is striking. Another difference is that Fig. 9 shows practically no dependence on the sediment model, while this dependence is pronounced in Fig. 10. Finally, note that the zero-crossing offset is absent from the month-to-month variations in Fig. 9. Empirical orthogonal function analysis of the transport streamfunction in the region around the cable shows that the dominant patterns have timescales of several months up to the full 2 years and largely represent wobbles and changes in the strength of the nearshore features. All of this indicates that the offset and misfit have the same source: the steady and slowly fluctuating aspects of the semipermanent eddy or recirculation over the model slope and the division between the shoreward and deeper branches of the model ''Gulf Stream.'' As mentioned already, the CME model differs notably from the real world in the imperfect separation of its Gulf Stream from the coast (cf. Figs. 2, 6, and 7). Part of the transport is trapped on the landward side of a large, semipermanent eddy or recirculation, while another branch lies in much deeper water, closer to the actual Gulf Stream path. Recirculations are an important part of the western boundary current system, but the CME version is clearly dissimilar from the picture emerging from experimental work (see Johns et al. 1995 for a recent synthesis of array measurements in the region). Because of its broader distribution of the flow across the continental margin, the model seems likely to be biased toward large meandering effects.

In summary, we find the voltage–transport linearity of the model Bermuda cable very good for the month-to-month changes dominated by variability over the offshore end. For the longer periods, from several months up to the full 2 years we analyzed, the CME model's incomplete Gulf Stream separation and slowly evolving nearshore recirculation prevent a quantitative estimate. To address this further, calculations based on more realistic ocean models are needed, especially to understand longer period variations and the influence of more realistic activity over the continental slope. At present, we can say that the problems of meandering effects when recirculation gyres shift over the continental margin, and of transport wandering off the cable end are likely to be overestimated by the CME model.

7. Other North Atlantic cables

We now present simulated voltage–transport linearity results for a number of other North Atlantic cables. The

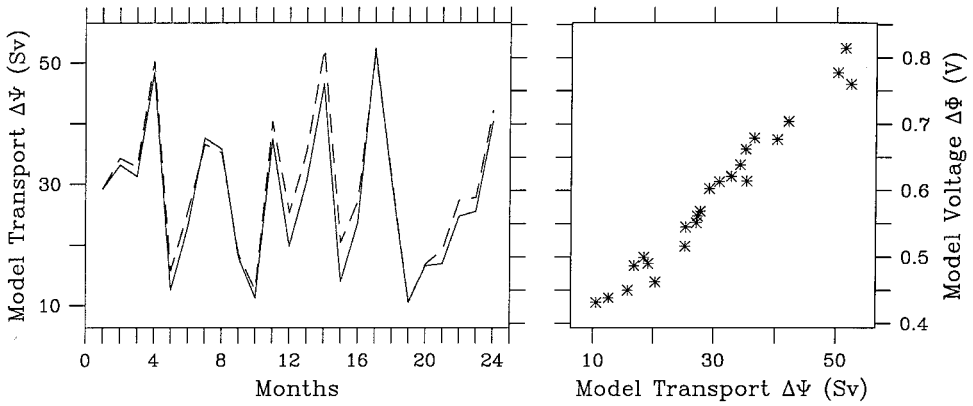

FIG. 8. (a) Simulated two-year time series for transport (dotted) and voltage (solid) across the deep water Bermuda cable. The voltage is assumed to be measured between points about 100 nautical miles offshore. In practice, this would be done with a seafloor voltmeter on one end. An arbitrary multiplicative factor (not chosen for the best possible fit) has been used to get the two curves on the same plot. For simplicity, only the voltage time series corresponding to the more conductive of the two sediment profiles is shown. (b) Simulated voltage–transport relationship of CME model transport fluctuations and computed voltage differences for the deep-water Bermuda cable. The nonzero intersect is due to the interplay of the bathymetry and the mean flow. It is larger in the model than would be expected in reality because of the large and nearly stationary nearshore flow in the CME model (cf. Figs. 6 and 7) and will be experimentally indistinguishable from electrode biases or electric currents from the earth's core.

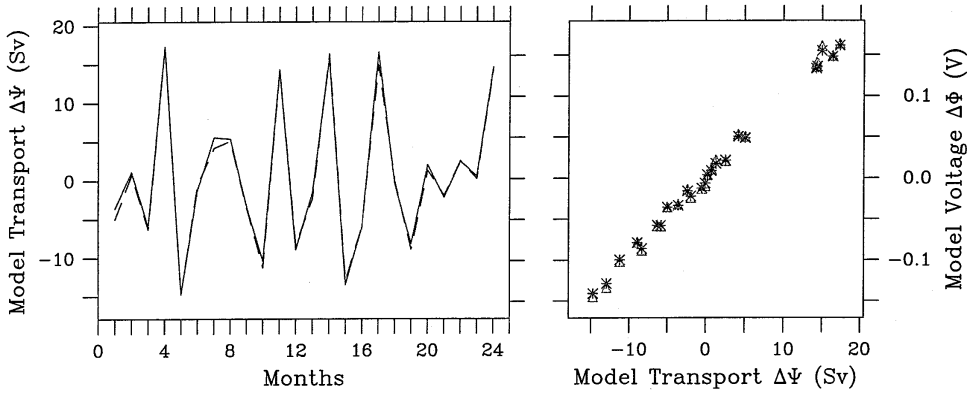

FIG. 9. As in Fig. 8 after the 3-month boxcar running average has been removed. Stars: the less conductive sediment model; triangles: the more conductive model.

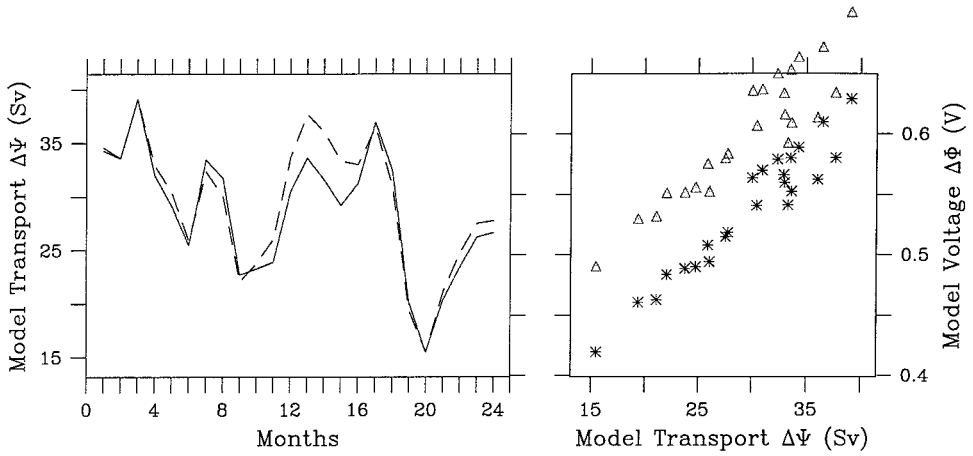

FIG. 10. As in Fig. 8 after a 3-month boxcar running average. Stars: the less conductive sediment model; triangles: the more conductive model.

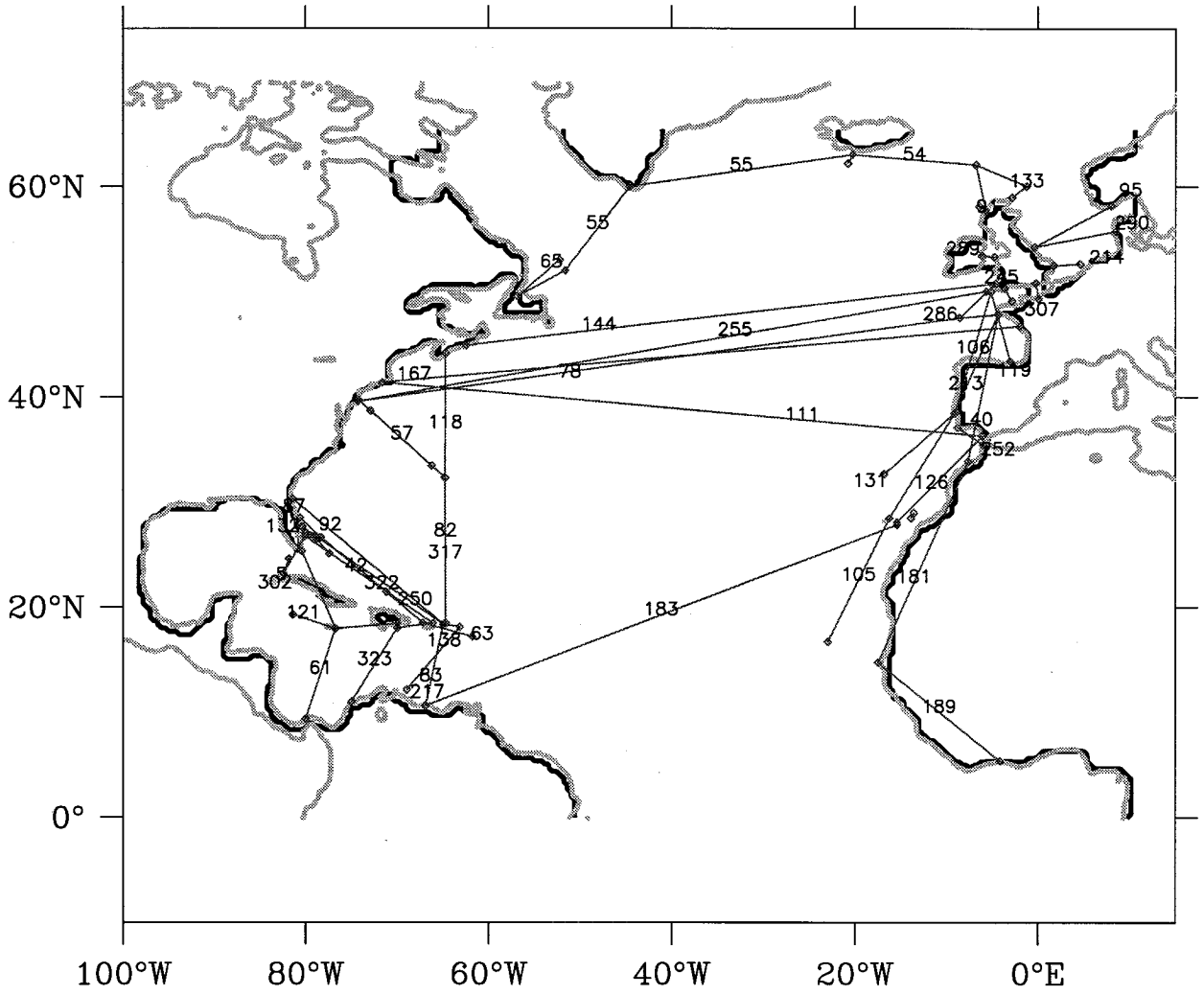

FIG. 11. Map showing cable endpoints as used in our calculations. The endpoints are connected by straight lines labeled by cable number as in the NTIA cable handbook (U.S. Department of Commerce 1991) and Tables 3–5. The CME model coastline is indicated by a heavy line and the higher resolution ETOPO-5 coastline by a lighter line. Note that due to poor resolution of islands and peninsulas, cable ends as entered from the cable handbook are sometimes a considerable distance offshore in the model.

cable information is drawn from the U.S. Department of Commerce (1991) ''World's Submarine Telephone Cable Systems'' handbook. The cables we used are shown in Fig. 11. The endpoint coordinates are connected by straight lines and labeled by the cable handbook number. A number of cables were left out for clarity, especially transatlantic and coastal cables of which there were already several examples, and cables newer than 1990 are not listed. The condition of many of the older cables we have included is uncertain, and in many cases cable ends are located on headlands or islands, which are represented by offshore locations or shallow plateaus in the CME model. With the exception of the Florida and Bermuda cables, however, we have for simplicity done the calculations in Tables 3 and 4 using the full, nominal lengths and endpoint coordinates. For these reasons, and because of the shortcomings of the ocean model, the tables in this section should be taken as rough indications rather than as the last word on particular cables.

The voltage and transport fluctuations shown in Tables 3–5 were obtained by the procedure already used for the Straits of Florida and Bermuda cables. At each step of the simulated 24-month simulated time series, a net transport value was computed by interpolating the transport streamfunction values to the cable end coordinates, then taking differences. The mean transport sign was chosen so that for cables oriented predominantly in the E–W direction, positive corresponds to northward transport, and for predominantly N–S cables, it means eastward transport. Voltages were computed similarly, by differences of interpolated electric potential values. The results shown are the average of results using the two sediment models. Errors, evident for instance in the

TABLE 3. Voltage–transport relationship for a selection of North Atlantic cables with nonvanishing net volume transport fluctuations in the CME model. The first column gives each cable's reference number in the NTIA cable handbook (U.S. Dept. Commerce 1991). The next column lists a brief summary of information about each cable, including the endpoint locations (see also Fig. 13), the cable's years of operation as of the 1990 handbook, the cable type, abbreviating coaxial by ''C,'' armored coaxial by ''AC,'' optical by ''O,'' and military by ''M,'' and the cable's name or acronym, when reasonably short. The remaining columns are obtained from the CME model by the procedure described in the text. A few notes: 1) First listed is the retired cable used for transport measurements in the Straits of Florida at 27°N between 1981 and 1990. It lacks a handbook number, being one of the many shorter, repeaterless cables not listed in the handbook. 2) Cable 132 is the in-service cable now in use for continuation of the 27°N time series. 3) Cable 302 consists of a recycled portion of the old transatlantic cable TAT-3.

NTIA cable number	Ends, (years active as of 1990), cable type, [acronym]	Corr. coeff. sqd r^2	Voltage rms fluct. (mV)	Transpt rms fluct. (Sv)	Transpt rms misfit (Sv)	Transpt mean (Sv)
0	Jupiter Break–Grand Bahama, (73-), C, [Bahamas-1]	.98	50.	1.5	.2	17.5
5	Key West–Havana, (50–89), AC	.98	49.	1.9	.3	19.7
54	S-Iceland–Faeroes, (62–87), AC, [SCOTICE]	.75	21.	.3	.1	−2.3
54	Faeroes–Scotland, (62–85), AC, [SCOTICE]	.85	50.	.3	.1	2.7
55	Newfndlnd–Break, (62–87), AC, [ICECAN]	.96	76.	.8	.1	−2.8
55	Break–S-Greenland, (62–87), AC, [ICECAN]	.45	19.	.8	.6	−2.8
57	New Jersey–Bermuda, (62–87), C, [BER-1]	.83	73.	6.7	2.8	30.4
57	deep offshore only	.96	108.	11.6	2.4	29.9
61	Florida–Jamaica, (63-), C	.87	93.	3.6	1.3	20.3
61	Jamaica–Panama, (63-), C	.70	56.	3.6	2.0	−20.3
63	Grand Turk–Puerto Rico, (63–86), AC	.70	10.	.9	.5	−6.1
63	Puerto Rico–Antigua, (63–86), AC	.73	12.	.9	.4	−5.0
83	Virgin Isl–Venezuela, (66–87), C	.58	23.	1.9	1.3	−14.9
87	Florida–Grand Bahama, (67–87), CM	.93	70.	2.1	.5	21.8
87	Grand Bahama–Grand Turk, (67–87), CM	.04	21.	.6	.6	−1.2
91	Scotland–Stornoway, (67–83), AC	1.00	23.	.07	0.00	.35
92	Florida–Virgin Isl, (68-), C, [STT2]	.57	64.	2.0	1.3	14.9
105	Portugal–Canary Isl, (69-), C	.95	23.	1.6	.3	1.6
105	Canary Isl–Cape Verde, (69-), C	.80	32.	4.5	2.0	−3.0
118	Nova Scotia–Bermuda, (71–90), C, [CANBER]	.47	87.	6.7	4.8	30.4
120	Canaries–Canaries, (71-), C, [TRANSCAN]	.96	3.	.3	.1	−.3
121	Grand Cayman–Jamaica, (71-), C	.85	45.	2.7	1.0	−2.0
126	Spain–Canaries, (71-), C, [PENCAN-2]	.90	16.	.9	.3	−.5
131	Lisboa–Madeira, (72-), C, [CAM-1]	.96	27.	2.5	.5	1.6
132	Florida–Grand Bahama, (73-), C	.99	63.	2.1	.2	22.0
132	Grand Bahama–Nassau, (73-), C	.07	15.	.2	.2	−.3
133	Orkney–Shetlands, (71-), AC	.99	31.	.2	0.0	−1.0
133	Shetlands–Faeroes, (71-), AC	.44	14.	.1	.1	1.1
138	Virgin Isl–N Antilles, (73-), C	.94	11.	.7	.2	−5.0
138	N Antilles–Curacao, (73-), C	.76	26.	3.0	1.5	−10.0
183	Canaries–Venezuela, (77-), C, [COLUMBUS]	.13	22.	.8	.7	.3
217	Virgin Isl–Venezuela, (80-), C, [VENEZ-2]	.58	23.	1.9	1.3	−14.9
245	England–Jersey, (82-), AC	.98	11.	.03	.01	−.05
72 250	Florida–Virgin Isl, (83-), C, [STT3]	.59	67.	2.0	1.3	14.9
302	Florida–Cuba, (0), C, [US-Cuba-7]	.93	60.	2.0	.5	19.8
82 317	Bermuda–Tortola, (90-), C, [CARAC]	.92	74.	6.7	1.9	−15.5
42 322	Florida–Puerto Rico, (90-), O, [FLORICO]	.63	63.	1.9	1.2	14.9

not-quite zero transport values in Table 4, may be due to numerical errors in the electric potential or interpolation errors in the streamfunction. They can also be due to poor model resolution of cable landing sites, especially in the common case of cable ends situated on unresolved islands or headlands. We have already seen an example of this uncertainty in the Straits of Florida at 27°N (Table 1). For another example note the offshore model location of ''Havana'' at the end of cables 5 and 132 (Fig. 11).

For clarity, we break up the numerical results into two separate tables. Results for cables with significant volume transport fluctuations are shown in Table 3. Many of the cables in the table show poor voltage–transport correlations. Among the likely reasons are near-closed circulations (e.g., cable 183, COLUMBUS), transport over extensive shelf and slope regions (e.g., cable 118, CANBER), and poor resolution of very short cables (several Caribbean cables). However, in addition to the Jupiter and Bermuda cables, already discussed in some detail, the table shows a number of cables with very linear voltage–transport relationships. Among these, there are examples in the open ocean (e.g., cable 317, CARAC, between Bermuda and Tortola); quite close to the northern boundary of the ocean model (cable 54, SCOTICE, between Scotland and the Faeroes, Fig. 12); and near the eastern boundary (cables 105, SAT 1; 126, PENCAN; and 131, CAM 1 between the Iberian peninsula and islands off northern Africa, Fig. 13).

Table 4 shows the rms voltage fluctuations for a num-

TABLE 4. Voltage and transport fluctuations for cables with nearly vanishing net volume transport. For some of the examples in this table, the reason for zero transport fluctuations is that the cable begins and ends at the same coastline (e.g., Antinéa and Fraternité between points on the west coast of Africa, TAGIDE between points on the European continent, the unbroken ICECAN across the Labrador Sea). In other cases, the transport very nearly vanishes because a closed circulation is straddled, either in a horizontal plane (e.g., TAT-5 across the North Atlantic) or in a vertical plane (e.g., ATLAS across Gibraltar). Due to boundary conditions and model limitations, this is the case for more cables in the model than would be the case in the real world (Denmark Strait and the English Channel, for instance).

NTIA Cable No.	Ends, (Years active as of 1990), Cable type, [ACRONYM]	Voltage rms fluct. (mV)	Transpt rms fluct. (Sv)	Transpt mean (Sv)
55	S-Greenland–S-Iceland, (62–87), AC, [ICECAN]	13.	0.0	−.4
78	France–New Jersey, (65–86), C, [TAT-4]	36.	.0	.0
95	S-Norway–Yorkshire, (68–88), AC	98.	.0	.0
106	SW-England–Portugal, (69-), C	12.	0.0	0.0
111	Rhode Isl–Spain, (70-), C, [TAT-5]	41.	.0	.0
119	SW-England–N-Spain, (70-), C, [UK-SP-1]	13.	0.0	0.0
140	France–Casablanca, (73-), C	13.	0.0	0.0
144	Cornwall–Nova Scotia, (74-), C, [CANTAT-2]	44.	.0	.0
167	France–Rhode Island, (76-), C, [TAT-6]	44.	.0	.0
181	Casablanca–Dakar, (77-), C, [Antinéa]	32.	.1	−.1
189	Dakar–Abidjan, (78-), C, [Fraternité]	27.	.1	.1
213	Portugal–France, (79-), C, [TAGIDE]	10.	.0	.0
214	Suffolk–Netherlands, (79-), AC	27.	.0	.0
252	Portugal–Morocco, (82-), C, [ATLAS]	2.	.0	.0
255	Land's End–New Jersey, (83-), C, [TAT-7]	37.	.1	0.0
289	Wales–Ireland, (88-), O, [UK-Ireland-1]	3.	.0	.0
290	Yorkshire–Denmark, (88-), O, [UK-Denmark-4]	94.	.0	.0
307	Brighton–Dieppe, (79-), AC, [UK-France-3]	3.	.0	.0

ber of cables that straddle nearly closed circulations so that they have vanishing or near-vanishing transport fluctuations. In that case, a net volume transport interpretation is clearly impossible. In some of the cases, the net transport vanishes due to real world constraints; for instance for cables connecting points on the same coastline or spanning a closed basin. In other cases, the constraints are due to the CME model's boundary conditions or other limitations, for instance in the Denmark Strait, Strait of Gibraltar, and the English Channel. The table shows that, even when net transports vanish, there are generally quite sizeable voltage fluctuations. The reasons include the weighting of the flowfield by the local seawater temperature and salinity, and by the spatially varying geomagnetic field, the influence of topographic and sediment cover variations, and electric current loops. The possibilities of alternative oceanographic interpretation, for instance in terms of heat and salt flux for exchange flows, will be left to future work and not discussed further here. We will, however, look at some examples of using less than the full cable length.

There are a number of situations in which the voltage over part of a cable might be useful. Many of the newer fiber optic cables have branching units with one of the branches grounded at sea. The possible measurements may include one coast–coast voltage as well as the voltage differences over the remaining spurs from the branching unit to shore. The quality of the observations will depend on how successfully the voltage drop associated with the power current can be removed (Larsen 1991). As a favorable example, we show simulated results for the ~ 80 km spur of fiber optic cable CANTAT-3, installed recently into Vestmannaeyjar, south of Iceland (an approximate branch location is used for the results in the table). The time series corresponding to this entry are shown in Fig. 14. For a less favorable example, we also tabulate the model-derived calibration results for each of the relatively short spurs of cable 286 (TAT-8), the fiber optic cable used by Medford et al. (1989), into Western Europe. For older, now retired cables cut at sea, the high cost of cable repairs may mean that seafloor-based measurements of voltage differences across portions of the cable are the only remaining option for scientific use. The example of the Bermuda cable has already illustrated that using only the deeper part of a cable may improve the voltage–transport correlation and reduce the dependence on sediment conductance. As a different type of example, in Table 5 we show results for the two segments of the now broken ICECAN between Newfoundland and Greenland. This cable had long been vulnerable to intensive fishing activity on the shelf break off Newfoundland. It was decommissioned in 1987, and the break off Newfoundland has been approximately located by resistance measurements from shore. Voltage measurements have been attempted on the Newfoundland shelf segment of this cable, but have proved difficult because of the remote location, severe weather, and proximity to the auroral zone.

8. Practical considerations—The case for seafloor-based monitoring

At present, retirement of older and now obsolete cables is proceeding at a great rate. Shore access is being lost both due to factors such as fishing activity and due

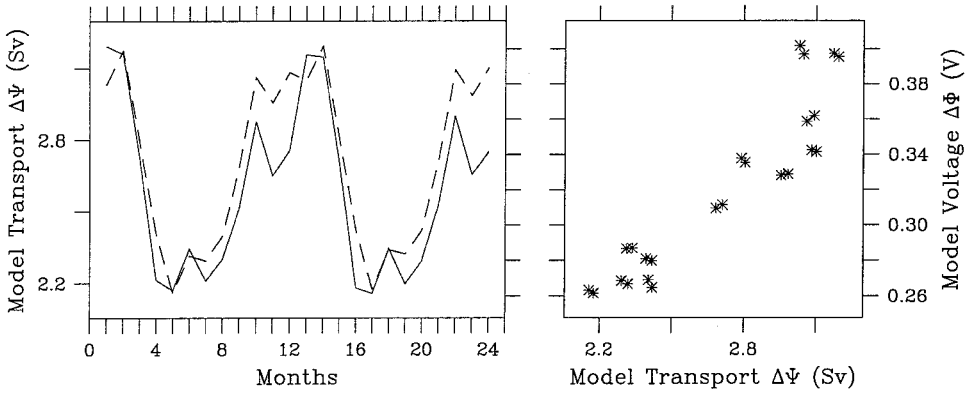

FIG. 12. Simulated voltage–difference transport relationship for cable 54 between Scotland and the Faeroes. For simplicity, only the voltage time series corresponding to the more conductive of the two sediment profiles is shown.

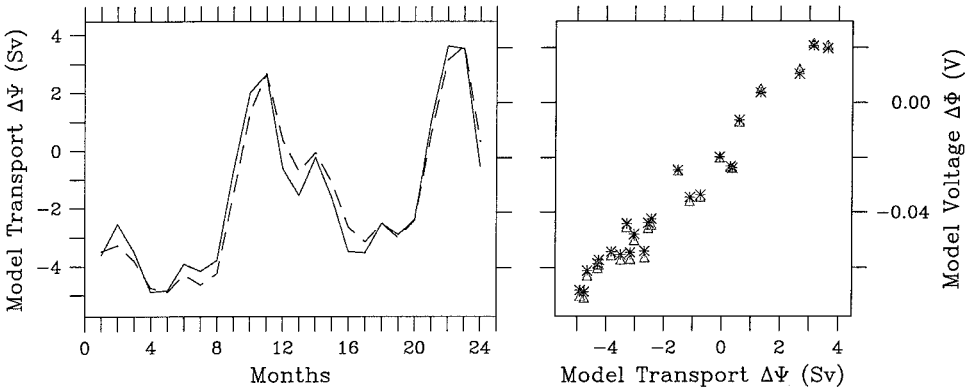

FIG. 13. Simulated voltage difference–transport relationship for cable 131 between Lisboa, Portugal, and the island of Madeira. Both sediment conductivity models can be shown without cluttering the figure since the response is practically independent of the sediment model.

to the interests of cable owners. In the case of commercial telecommunication companies these include liability concerns and reuse of favored landing approaches and beach sites, and in the case of the military, budgetary, and security concerns. For instance, in the past two years, shore access of ICECAN and SCOTICE has been lost in Iceland due to reuse of the landing site for a new fiber optic cable, the shore access of several of AT&T's transatlantic cables either already has been or is likely to be lost, and there have been doubts as to the future of the U.S. Navy cables.

While maintaining shore access is thus problematic, many of the activities that cause cable removals and breaks are concentrated in the nearshore regions. Even with all or almost all shore facilities of the current generation of cables gone, we can expect that for decades, the deep-sea portions of these cables will still be in good condition. For these, 60-year lifetimes are not unrea-

TABLE 5. Model results for portions of cables that straddle closed circulations.

NTIA Cable No.	Ends, (Years active as of 1990), Cable type, [ACRONYM]	Corr. coeff sqd r^2	Voltage rms fluct. (mV)	Transpt rms fluct. (Sv)	Transpt rms misfit (Sv)	Transpt mean (Sv)
	Canada to N. Europe, (94-), O, [CANTAT-3]					
	S-Iceland–Branch ~80 km SSE	.98	12.	.3	0.0	−4.2
286	New Jersey–England, France, (88-), O, [TAT-8]					
286	Branchpoint–Cornwall, (88-), O	.62	16.	.2	.1	.2
286	Branchpoint–France, (88-), O	.63	13.	.2	.1	.2
55	Newfndlnd–S-Greenland, (62–87), AC, [ICECAN]					
55	Newfndlnd–Break	.96	76.	.8	.1	−2.8
55	Break–S-Greenland	.45	19.	.8	.6	−2.8

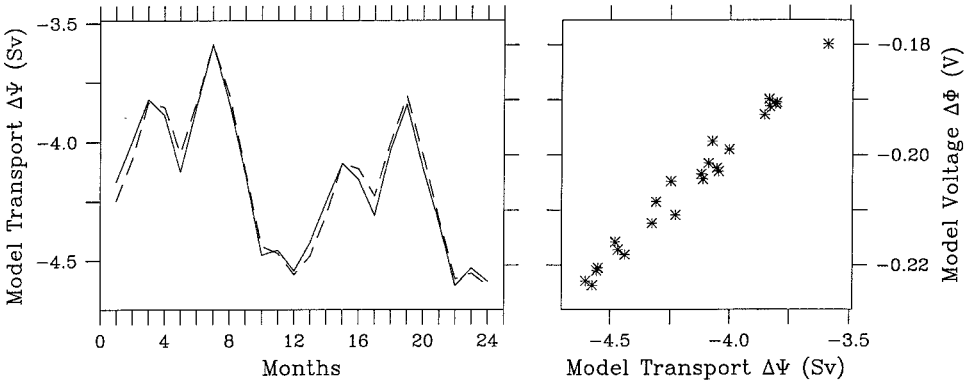

FIG. 14. Simulated voltage difference–transport relationship for the ~80 km spur of fiber optic cable CANTAT-3 installed last year Vestmannaeyjar, south of Iceland. The approximate branchpoint location used for the computation corresponds to a cable about 100 km long. To avoid cluttering the figure, only the voltage time series corresponding to the more conductive of the two sediment profiles is shown.

sonable; the oldest telegraph cables lasted from 1864 to 1946, and some of the generation of telegraph cables laid just after the turn of the century were in use past 1960. We believe that in many cases the best approach will be to install underwater instrumentation offshore. This has several advantages. One is a more stable electrode environment than well- or beach-based contacts. For accuracy, there will also be an advantage since meandering effects tend to be reduced for the deep water portions of cables and geophysical uncertainties will be less important. In any case, oceanographic interpretation is made easier by measuring shallow and deep water transports separately. There may, however, be trade-offs associated with a shorter length if meandering of transport past the cable ends makes interpretation less clear. Finally, the larger choice of cables available if shore access is not required means that the scientific options are wider. Apart from the as yet largely untested possibilities of fiber optic cables, seafloor-based instrumentation near shelfbreaks or even in deep water may provide the most reliable opportunities for long-term monitoring of large-scale net transports.

9. Discussion

We have applied our flow-induced voltage model to a number of active and retired cables in the North Atlantic. The main result has been to show that a linear relationship between voltage and net cross-cable mass transport can prevail over large distances, even with complex flow patterns, realistic topography, and earth models. In many cases, effects of flow meandering, variable seawater temperature and salinity, and large-scale electric currents thus appear less severe than had been feared. Although a certain amount of data scatter will result from these effects, this should be put into perspective by the analogous errors introduced into other types of transport measurements, for instance by meanderings past arrays of point measurements or by scales missed between moorings or satellite tracks.

Submarine cables are designed for a long working life and can last for decades. With a combination of luck and persistence, the Florida Current time series has proved cable measurements capable of yielding long, continuously sampled time series. The large day-to-day fluctuations seen there exemplify the danger of temporal aliasing from intermittent measurements. Continuous cable time series can also offer the possibility of tying together less continuous measurements made by other methods. This can make it possible to put discrete data or individual surveys in the context of a long time series.

The natural integration properties of cable voltages have both advantages and disadvantages. The integration means that the spatial distribution of the signals is lost both in the vertical and along-cable directions, so that cable voltages do not, except for second-order effects, distinguish between a closed circulation and a state of rest. However, for the problem of trying to monitor the large-scale net transports, this constitutes an advantage. Eddies, planetary waves, and recirculations that require great effort to resolve with point measurements are naturally integrated out by appropriately located cables. The vertical integration means that they sense the full flow field.

The simulation presented here indicates that many cables exist or have existed for which voltage fluctuations are dominated by net transport fluctuations. The results confirm that long open-ocean cables are much less sensitive to uncertainty in sediment conductivity than is the case in the shallow, heavily sedimented Straits of Florida. In the straits, the numerically derived calibration factor matched the empirical value within 25%, as well as could be expected given the uncertainty in the conductance of the thick pile of local sediments and the imperfect resolution of the straits. Based on this, we expect that in many cases, numerical models will be usable for a reasonable first estimate of calibration factors. Of course every opportunity should be taken to check and refine these experimentally. Use of higher

resolution topography, more local geological information, and improved ocean models will also check and narrow down model-derived calibration factors. In view of the importance of long-term, large-scale net transport monitoring, and the difficulty of accomplishing this task by other methods, we believe that carefully chosen large-scale voltage observations hold much promise and should be explored through renewed modeling, observation, and interpretation efforts.

Acknowledgments. The authors thank C. S. Cox for suggesting the circulation model approach, for many valuable discussions, and for the inspiration of his example over the years. We also thank A. D. Chave, B. D. Cornuelle, E. Gottlieb, D. S. Luther, T. Rossby, T. B. Sanford, V. Shneyer, and G. Spence for useful discussions; F. Bryan for providing the depth-integrated WOCE Community Modeling Effort results; and A. Manke and D. McClurg for programming support. A. D. Chave and an anonymous reviewer are thanked for comments that have greatly improved the paper. We are indebted to NSF Grant OC90-19314, the National Research Council, and NOAA's Atlantic Climate Program for supporting this work.

APPENDIX

Cable Calibration, Simple Estimates

Both as a check on the numerical results and for the sake of physical intuition, it is of interest to be able to estimate bounds on calibration factors from simple approximations without the use of numerical models or site-specific data. To do this, we need to estimate the ratio of the two along-cable integrals (3) and (4):

$$\text{calibration factor} = \frac{\text{voltage difference}}{\text{volume transport}} = \frac{\int E_{\|}\, dl}{\int \int_{\text{sea}} v_{\perp}\, dz\, dl}.$$

This form does not make simple estimates particularly easy. However, the local ratio of the integrands can be estimated using an approximate relationship between the local transport per unit width and horizontal electric field (e.g., Sanford 1971; Chave and Luther 1990). This approximation assumes long wavelengths and neglects large-scale electric current effects. Formally, it is equivalent to integrating Ohm's law, $\mathbf{j} = \sigma(\mathbf{E} + \mathbf{v} \times \mathbf{F})$, over depth through the sea and seabed and neglecting the left-hand side. The ''local calibration factor'' can then be expressed as

$$\Lambda = \frac{E_{\|}}{\int_{\text{sea}} v_{\perp}\, dz} = \frac{\int_{\text{sea}} \sigma \mathbf{v}\, dz \times F_z}{\left[\int_{\text{sea+seabed}} \sigma\, dz\right]\left[\int_{\text{sea}} \mathbf{v}\, dz\right]}. \quad \text{(A1)}$$

This ratio may not always be a good way to approach the question of a given cable's sensitivity; for instance, it becomes meaningless in situations where the denominator vanishes. However, it provides a straightforward way to convert information about the local geology, geophysics, effective flow location, temperature, and salinity into a calibration factor estimate. Furthermore, its along-cable variation can be used to assess the importance of meandering effects. In this section we illustrate a rough, back-of-the-envelope approach to doing this. A detailed experimental approach is also possible, and has been illustrated by Spain and Sanford (1987) in the Straits of Florida at 27°N. They used Pegasus and XCP profiling data taken along a line slightly north of the Jupiter cable to construct careful estimates of the constituent parts of (A1).

In a form suitable for making simple estimates, the local ratio Λ may be written in a notation similar to that of Spain and Sanford as

$$\Lambda = \frac{(1 + \gamma)}{(1 + \lambda)} \frac{F_z}{H_{\text{sea}}}. \quad \text{(A2)}$$

In this expression, F_z is the local geomagnetic field and H_{sea} is the water depth. The factor λ accounts for electric shorting with return current loops split between two conductors in parallel; the seawater column and the seabed (e.g., Sanford and Flick 1975). It is given by $\lambda = \int_{\text{seabed}} \sigma\, dz / \int_{\text{sea}} \sigma\, dz$. Its value is on the order of 1 in the Straits of Florida, but is only a few percent on the deep sea floor. The factor $(1 + \gamma)$ represents the influence of seawater conductivity variations. For simple estimates, it can be thought of as the ratio of the effective conductivity to the average over the full water column. Formally, it can be expressed as the ratio of the velocity-weighted to the depth-averaged conductivity (Larsen 1992). Alternately, γ can be expressed, using Sanford's notation, as $\gamma = \overline{\sigma' v'} / \overline{\sigma v}$, the bar denoting a depth average and the prime the depth-varying part of a Reynolds decomposition. This effect is at its greatest for highly baroclinic currents concentrated in warm, saline water overlying a deep water column, where it can be as much as one-third. It is small, however, over much of the ocean (see the estimates of Luther and Chave 1993) and vanishes where either the velocity or conductivity is independent of depth.

To illustrate the sort of assumptions that can be used for back-of-the-envelope estimates of calibration factors and their along-cable variation without the use of numerical models or local data, we will now estimate bounds on both the Florida Straits calibration factor and on the open-ocean example discussed in the text; a cable crossing the North Atlantic margin and the western boundary currents.

a. Straits of Florida at 27°N

Taking Fig. 4 as a guide, [400–700] m should comfortably bracket any reasonable effective depth for flow

through the straits. Seabed shorting due to sediments in the straits is a first-order influence on the strait calibration factor. Trying to estimate bounds on sediment conductance without reference to data specific to this location, we might estimate a reasonable range of sediment conductivities as $\sigma_{sed} = [0.2–2]$ S m^{-1} for the uppermost km of sediments and [0.05–0.5] S m^{-1} for the deeper 3 km of sedimentary layers. Our generous bounds on the sediment conductance in the sediment column in the straits would then be [350–3500] S [the experimental values of Spain and Sanford (1987) and Larsen (1992) are on the order of 2800 and 1900 S, respectively]. The flow-conductivity factor γ is not very large in the straits, mainly due to the absence of a deep underlying water column. Larsen's (1992) estimate of a flow-weighted conductivity of 4.8 S m^{-1} and a depth-averaged conductivity of 4.6 S m^{-1} is in good agreement with Spain and Sanford's (1987) value of $\gamma \approx 5\%$. We will assume $\bar{\sigma}_{sea} = 4.6$ S m^{-1} in the estimate of λ, and to err on the side of generous bounds, take $\gamma = 5 \pm 5\%$.

For an upper-limit calibration factor estimate, taking the higher value for γ, the shallower effective water depth, and λ consistent with this depth and the lower-bound sediment conductivity yields

$$\lambda = \frac{0.2 \text{ S/m}^{-1}\cdot 1000 \text{ m}^{-1} + 0.05 \text{ Sm}^{-1}\cdot 3000 \text{ m}}{4.6 \text{ Sm}^{-1}\cdot 400 \text{ m}} = 0.2$$

$$\Lambda^{\text{upper}}_{\text{limit}} = \frac{1.1}{1+0.2}\frac{41\,100 \text{ nT}}{400 \text{ m}} = 94 \text{ mV Sv}^{-1}.$$

On the other hand, choosing the lower value for γ, the deeper effective water depth H_{sea} and λ based on this water depth, and the more conductive sediment values yields

$$\lambda = \frac{2\text{S m}^{-1}\cdot 1000\text{m} + 0.5 \text{ S m}^{-1}\cdot 3000\text{m}}{4.6\text{S m}^{-1}\cdot 700\text{m}} = 1.9$$

$$\Lambda^{\text{lower}}_{\text{limit}} = \frac{1.0}{1+1.9}\frac{41,100 \text{ nT}}{700\text{m}} = 20\text{mV Sv}^{-1},$$

where Sv$^{-1} \equiv 10^6$ m^3 s^{-1}. By these very crude estimates, the actual Florida Straits calibration factor of 40.9 mV Sv^{-1} is bracketed by $\Lambda = [20–94]$ mV Sv^{-1}, illustrating that even extremely rough estimates, ignoring the wealth of information available at this specific location, can bracket the range of possible calibration factor values to within a factor of 2. As illustrated by the next section, the uncertainty due to the seabed shorting will be much less in deeper water, while that due to the effective flow-conductivity takes on a greater role.

b. New Jersey–Bermuda cable, deep water

We now use similar assumptions to estimate bounds on the calibration factor for the New Jersey–Bermuda cable. We will use the sediment conductivity bounds unchanged. For an upper bound on the flow-conductivity factor, we will use estimates based on conductivity–velocity profiles by Sanford and coworkers (Dunlap et al. 1992) about 200 km downstream of the Woods Hole–Bermuda line, where they found $\gamma = 37\%$ for the Gulf Stream in deep water. This value can be extrapolated to the Gulf Stream over shallower water by the method of Dunlap et al. (1992), cutting off the deeper part of the velocity and conductivity profiles before γ is computed. Since parts of the flow field may be characterized by more barotropic flow or by smaller depth-variations of temperature and salinity, the cable's effective value of γ for the cable may be lower than this. As an extreme lower bound on the flow-conductivity factor, we will use $\gamma = 0$.

We begin with an estimate of a lower-limit calibration factor. For a self-consistent estimate, we estimate the water depth, sediment thickness, and vertical magnetic field at the same location, say at approximately 35°N, the deepest section of the cable. Here $F_z = 48\,000$ nT, $\bar{\sigma}_{sea} = 4$ S m^{-1}, $H_{sea} = 5000$ m, and $H_{sed} = 700$ m are reasonable numbers. Since this is to be a lower limit, we use $\gamma = 0$, and

$$\lambda = \frac{2 \text{ S.m}^{-1}\cdot 700 \text{ m}}{4 \text{ S/m}^{-1}\cdot 5000 \text{ m}} = 0.07$$

$$\Lambda^{\text{lower}}_{\text{limit}} = \frac{1.0}{1 + 0.07}\frac{48\,000 \text{ nT}}{5000 \text{ m}} = 9 \text{ mV Sv}^{-1}.$$

For an upper limit applicable over the deep-water stretch, we repeat this estimate closer to the coast, near where the cable crosses 38°N. Here we will take $F_z = 51\,000$ nT, $\bar{\sigma}_{sea} = 4$ S m^{-1}, $H_{sea} = 3000$ m, and $H_{sed} = 5000$ m. The least conductive sediment values give $\lambda = 0.007$. For an upper-limit γ, we follow Dunlap et al.'s (1992) extrapolation of the Gulf Stream results used earlier to various depths of water by cutting off the part of the profiles below 3 km depth. This results in a value of $\gamma \approx 25\%$, so

$$\Lambda^{\text{lower}}_{\text{limit}} = \frac{1.25}{1 + 0.007}\frac{51\,000 \text{ nT}}{3000 \text{ m}} = 21 \text{ mV Sv}^{-1}.$$

Our estimated bounds are then

$$\Lambda = [9–21] \text{ mV Sv}^{-1}$$

for flow across the deep-water stretch of the Bermuda cable.

c. New Jersey–Bermuda cable, upper continental slope

Finally, we will estimate a range of calibration factors applicable for flow concentrated over the upper reaches of the continental slope. For this estimate we will use $F_z = 51\,500$ nT, $\bar{\sigma}_{sea} = 4$ S m^{-1}, and $H_{sea} = 1000$ m. The sediment thickness varies very rapidly in this region; we will use $H_{sed} = 8000$ m for this estimate. For γ, we will use a value of [0%–15%], the upper limit again based on Dunlap et al.'s (1992) extrapolation of

the Gulf Stream results to various depths of water. For a lower-limit calibration factor estimate we take $\gamma = 0$,

$$\lambda = \frac{2 \text{ S/m}\cdot 1000 \text{ m} + 0.5 \text{ S/m}\cdot 7000 \text{ m}}{4 \text{ S/m}\cdot 1000 \text{ m}} = 1.4$$

$$\Lambda^{\text{lower}}_{\text{limit}} = \frac{1.0}{1 + 1.4}\frac{51\,500 \text{ nT}}{1000 \text{ m}} = 22 \text{ mV Sv}^{-1}.$$

For an upper-limit calibration factor estimate, we take $\gamma = 15\%$, $\lambda = 0.14$ so that

$$\Lambda^{\text{upper}}_{\text{limit}} = \frac{1.15}{1 + 1.14}\frac{51\,500 \text{ nT}}{1000 \text{ m}} = 52 \text{ mV Sv}^{-1}.$$

For the upper reaches of the continental slope, we thus have

$$\Lambda = [22\text{–}52] \text{ mV Sv}^{-1}.$$

REFERENCES

Bloom, G. L., 1964: Water transport and temperature measurements in the eastern Bering Strait, 1953–1958. *J. Geophys. Res.,* **70,** 3335–3353.

Boening, C. W., F. O. Bryan, W. R. Holland, and R. Doescher, 1996: Deep-water formation and meridional overturning in a high-resolution model of the North Atlantic. *J. Phys. Oceanogr.,* **26,** 1142–1164.

Bryan, F. O., and W. R. Holland, 1989: A high resolution simulation of the wind and thermohaline circulation in the North Atlantic Ocean. *Proceedings of 'Aha Huliko' a Hawaiian Workshop,* Hawaii Institute of Geophysics, 99–115.

Bryan, K., 1969: A numerical method for the study of the circulation of the world ocean. *J. Comput. Phys.,* **4,** 347–376.

Bullard, E. C., and R. L. Parker, 1968: Electromagnetic induction in the oceans. *Sea,* **4** (18), 695–730.

Chave, A. D., and D. S. Luther, 1990: Low frequency motionally-induced electromagnetic fields in the ocean. Part 1: Theory. *J. Geophys. Res.,* **95,** 7185–7200.

——, ——, and J. H. Filloux, 1997: Observations of the boundary current system at 26.5°N in the subtropical North Atlantic Ocean. *J. Phys. Oceanogr.,* in press.

——, A. Flosadóttir, and C. S. Cox, 1990: Some comments on seabed propagation of ULF/ELF electromagnetic fields. *Radio Sci.,* **25,** 825–836.

——, D. S. Luther, L. J. Lanzerotti, and L. V. Medford, 1992: Geoelectric field measurements on a planetary scale: Oceanographic and geophysical applications. *Geophys. Res. Lett.,* **19,** 1411–1414.

Cox, C. S., J. H. Filloux, D. I. Gough, J. C. Larsen, K. A. Poehls, R. P. von Herzen, and R. Winter, 1980: Atlantic lithosphere sounding. *J. Geomagn. Geoelectr.,* **32** (Suppl. I), SI 13–SI 32.

Dunlap, J. H., R. G. Drever, M. A. Kennelly, and T. B. Sanford, 1992: Measurements of Gulf Stream transport with a towed transport meter (TTM2) on R/V *Oceanus* Cruise 216. Tech. Rep. APL-UW TR9209, Applied Physics Laboratory University of Washington, Seattle, WA, 40pp.

Emery, K. O., and E. Uchupi, 1984: *The Geology of the Atlantic Ocean.* Springer-Verlag, 1050 pp.

Filloux, J. H., 1987: Instrumentation and experimental methods for oceanic studies. *Geomagnetism,* J. Jacobs, Ed., Academic Press, 143–248.

Flagg, C., G. Schwartze, E. Gottlieb, and T. Rossby, 1997: Operating an acoustic Doppler current profiler (ADCP) aboard a container vessel. *J. Atmos. Oceanic Technol.,* in press.

Flosadóttir, A. F., J. C. Larsen, and J. T. Smith, 1997: Motional induction in North Atlantic circulation models. *J. Geophys. Res.,* **98:** 10 353–10 372.

Fofonoff, N. P., and R. C. Millard Jr., 1983: Algorithms for computation of fundamental properties of sea water. UNESCO Tech. Paper Marine Science 44, 53 pp. [Available from UNESCO, 7 Place de Fontenoy, 75700 Paris, France.]

Fujii, I., 1995: Geoelectric potential variations over a planetary scale. Ph.D. thesis, University of Tokyo, 103 pp.

——, L. J. Lanzerotti, H. Utada, H. Kinoshita, J. Kasahara, L. V. Medford, and C. G. Maclennan, 1995: Geoelectric power spectra over oceanic distances. *Geophys. Res. Lett.,* **22,** 421–424.

Gill, A., 1982: *Atmosphere–Ocean Dynamics.* Academic Press, 662 pp.

Gottlieb, E., T. Rossby, G. Schwartze, and P. Cornillon, 1994: The Oleander Project first-year results: Gulf Stream ADCP measurements from October 1992 to October 1993. *Proc. Principal Investigators Meeting of the Atlantic Climate Change Program,* Princeton, NJ, University Corp. Atmos. Res., 145–148.

Hellerman, S., and M. Rosenstein, 1983: Normal monthly wind stress over the world ocean with error estimates. *J. Phys. Oceanogr.,* **13,** 1093–1105.

Johns, W. E., T. J. Shay, J. M. Bane, and D. R. Watts, 1995: Gulf Stream structure, transport, and recirculation near 68°W. *J. Geophys. Res.,* **100** (C1), 817–838.

Lanzerotti, L. J., A. D. Chave, C. H. Sayres, L. V. Medford, and C. G. Maclennan, 1993: Large-scale electric field measurements on the earth's surface: A review. *J. Geophys. Res.,* **98,** 23 525–23 534.

Larsen, J. C., 1968: Electric and magnetic fields induced by deep sea tides. *Geophys. J. Roy. Astron. Soc.,* **16,** 47–70.

——, 1980: Electromagnetic response functions from interrupted and noisy data. *J. Geomagn. Geoelectr.,* **32** (Suppl. I), 89–103

——, 1989: Transfer functions: Smooth robust estimates by least squares and remote reference methods. *Geophys J.,* **99,** 645–663.

——, 1991: Transport measurements from in-service undersea telephone cables. *IEEE J. Oceanic Eng.,* **16,** 313–318.

——, 1992: Transport and heat flux of the Florida Current at 27°N derived from cross-stream voltages and profiling data: Theory and observations. *Philos. Trans. Roy. Soc. London,* **338,** 169–236.

——, and T. B. Sanford, 1986: Florida Current volume transports from voltage measurements. *Science,* **227,** 302–304.

——, R. L. Mackie, A. Manzella, A. Fiordelisi, and S. Rieven, 1996: Robust smooth magnetotelluric transfer functions. *Geophys. J. Int.,* **124,** 801–819.

Leaman, K. D., R. L. Molinari, and P. S. Vertes, 1987: Structure and variability of the Florida Current at 27°N: April 1982–July 1984. *J. Phys. Oceanogr.,* **17,** 566–583.

Lilley, F. E. M., J. H. Filloux, N. L. Bindoff, I. J. Ferguson, and P. J. Mulhearn, 1986: Barotropic flow of a warm-core ring from seafloor electric measurements. *J. Geophys. Res.,* **91** (C), 11 979–12 984.

Longuet-Higgins, M. S., 1949: The electric and magnetic effects of tidal streams. *Mon. Not. Roy. Astron. Soc. Geophys.,* **5** (Suppl.), 285–307.

——, M. E. Stern, and H. Stommel, 1954: The electrical field induced by ocean currents and waves, with applications to the method of towed electrodes. *Pap. Phys. Oceanogr. Meteor.,* **13** (1), 37 pp.

Luther, D. S., and A. D. Chave, 1993: Observing ''integrating'' variables in the ocean. *Proceedings of the Seventh 'Aha Huliko' a Winter Hawaiian Workshop on Statistical Methods in Physical Oceanography,* Hawaii Institute of Geophysics, 103–130.

——, ——, and J. H. Filloux, 1991: Low frequency motionally induced electromagnetic fields in the ocean. Part 2: Electric field and Eulerian current comparison. *J. Geophys. Res.,* **96,** 12 797–12 814.

Medford, L. V., L. J. Lanzerotti, J. S. Kraus, and C. G. Maclennan,

1989: Transatlantic Earth potential variations during the March 1989 magnetic storms. *Geophys. Res. Lett.,* **16,** 1145–1148.

Petitt, R. A., A. D. Chave, J. H. Filloux, and H. H. Moeller, 1994: Electromagnetic field instrument for the continental shelf. *Sea Technol.,* **35,** 10–13.

Rikiishi, K., M. Michigami, T. Araki, K. Shiwaki, R. Eto, K. Taira, and J. Larsen, 1996: Cross-stream voltages induced by ocean currents in the Tsugaru Strait, northern Japan. *Extended Abstract, 13th Workshop on Electromagnetic Induction in the Earth,* Onuma, Japan, IAGA, 48.

Robinson, I. S., 1976: A theoretical analysis of the use of submarine cables as electromagnetic oceanographic flowmeters. *Philos. Trans. Roy. Soc. London,* **280** (1297), 355–396.

Runcorn, S. K., 1964: Measurements of planetary electric currents. *Nature,* **202,** 10–13.

Sanford, T. B., 1971: Motionally induced electric and magnetic fields in the sea. *J. Geophys. Res.,* **76,** 3476–3492.

——, 1982: Temperature transport and motional induction in the Florida Current. *J. Mar. Res.,* **40** (Suppl.), 621–639.

——, and R. E. Flick, 1975: On the relationship between transport and motional electric potentials in broad, shallow currents. *J. Mar. Res.,* **33** (Suppl.), 123–139.

——, R. G. Drever, and J. H. Dunlap, 1985: An acoustic Doppler and electromagnetic velocity profiles. *J. Atmos. Oceanic Technol.,* **2**, 120–124.

——, ——, ——, and W. E. Johns, 1995: Barotropic flows observed by the towed transport meter. *Proc. IEEE Fifth Working Conf. on Current Measurement,* S. Anderson, G. Appell, and A. J. Williams, III, Eds., Williams S. Sullwold Publishing, 24–29.

Smith, J. T., 1996a: Conservative modeling of 3-D electromagnetic fields: I. Properties and error analysis. *Geophysics,* **61,** 1308–1318.

——, 1996b. Conservative modeling of 3-D electromagnetic fields: II. Biconjugate gradient solution and an accelerator. *Geophysics,* **61,** 1319–1324.

Spain, P., and T. B. Sanford, 1987: Accurately monitoring the Florida Current with motionally-induced voltages. *J. Mar. Res.,* **7,** 843–870.

Stephenson, D., and K. Bryan, 1992: Large-scale electric and magnetic fields generated by the oceans. *J. Geophys. Res.,* **97,** 15 467–15 480.

Tarits, P., 1994: Electromagnetic studies of global geodynamic processes. *Surv. Geophysics,* **15,** 209–238.

Visscher, P. B., 1989: Discrete formulation of Maxwell equations. *Comput. Phys.,* **3,** 42–45.

U.S. Department of Commerce, 1991: World's submarine telephone cable systems. NTIA-CR-91-42. [Available from U.S. Govt. Printing Office, Washington, DC 20402.]

Webb, S. C., S. C. Constable, C. S. Cox, and T. Deaton, 1985: A seafloor electric field instrument. *J. Geomagn. Geoelectr.,* **37,** 1115–1130.